Report

Stress-related Noradrenergic Activity Prompts Large-scale Neural Network Reconfiguration

Erno J. Hermans[1,2,3*], Hein J.F. van Marle[1,4†], Lindsey Ossewaarde[1†], Marloes J.A.G. Henckens[1,5†], Shaozheng Qin[1,6†], Marlieke T.R. van Kesteren[1,7†], Vincent C. Schoots[1,8†], Helena Cousijn[1,9†], Mark Rijpkema[1,2], Robert Oostenveld[1], & Guillén Fernández[1,2]

1) Radboud University Nijmegen Medical Centre, Donders Institute for Brain, Cognition and Behaviour, 6500 HB, Nijmegen, The Netherlands
2) Radboud University Nijmegen Medical Centre, Department for Cognitive Neuroscience, 6500 HB, Nijmegen, The Netherlands
3) New York University, Department of Psychology, NY 10003, New York, USA
4) University of Amsterdam, Academic Medical Center, Department of Psychiatry, 1100 DD, Amsterdam, The Netherlands
5) University Medical Centre Utrecht, Rudolf Magnus Institute of Neuroscience, 3584 CG, Utrecht, The Netherlands
6) Stanford University School of Medicine, Department of Psychiatry and Behavioral Science, CA 94304, Stanford, USA
7) Radboud University Nijmegen Medical Centre, Department of Anatomy, 6500 HB, Nijmegen, The Netherlands
8) Erasmus University Rotterdam, Rotterdam School of Management, 3000 DR, Rotterdam, The Netherlands
9) Oxford University, Warneford Hospital, Department of Psychiatry, OX3 7JX, Oxford, United Kingdom

*To whom correspondence should be addressed. E-mail: erno.hermans@donders.ru.nl
†These authors contributed equally to this work.

Science, November 25, 2011
Vol. 334, Issue 6059, pp. 1151-1153
DOI: 10.1126/science.1209603

Acute stress shifts the brain into a state that fosters rapid defense mechanisms. Stress-related neuromodulators are thought to trigger this change by altering properties of large-scale neural populations throughout the brain. We investigated this brain state shift in humans. During exposure to a fear-related acute stressor, responsiveness and interconnectivity within a network including cortical (frontoinsular, dorsal anterior cingulate, inferotemporal, and temporoparietal) and subcortical (amygdala, thalamus, hypothalamus, and midbrain) regions increased as a function of stress response magnitudes. Beta-adrenergic receptor blockade, but not cortisol synthesis inhibition, diminished this increase. Thus, our findings reveal that noradrenergic activation during acute stress results in prolonged coupling within a distributed network that integrates information exchange between regions involved in autonomic-neuroendocrine control and vigilant attentional reorienting.

One-sentence summary

Acute stress leads to a reorganization of large-scale neural network connectivity in the brain that is driven by noradrenaline.

Acute stress alters the way our brain functions. This brain state shift can be understood as a strategic reallocation of resources to functions that are vital when survival is at stake: it sharpens our senses, creates a state of fearful arousal (1, 2), strengthens our memories of stressful experiences (3-5), but impairs our capacity for slow deliberation (6, 7).

Animal research into the acute stress response has delineated a chain of neurochemical events triggering the release of various hormones and neurotransmitters (1, 8). Acting as neuromodulators, these alter cellular properties of large-scale neuronal populations throughout the brain. Activation of the hypothalamic-pituitary-adrenal (HPA) axis, resulting in increased systemic release of corticosteroids, is the hallmark of the stress response. However, a host of central changes in neuropeptide and monamine release plays a key role at shorter time-scales (1, 5). For instance, acute stress elevates tonic firing rates in the locus coeruleus (LC), the primary source of noradrenaline in the forebrain (9-11), and corticosteroid effects in multiple brain regions depend on concomitant noradrenergic activation (4). We therefore hypothesized that stress-related neuromodulators, in particular noradrenaline, trigger brain state alterations by reorganizing neural activity within large-scale neuronal systems (12).

We tested this hypothesis in two experiments using model-free neuroimaging analyses that allow quantification of state changes during "real-world" experiences (13). To induce the intended change in a scanner environment while optimally preserving dynamic sensory and affective qualities of real-world threatening events, we exposed participants to highly aversive cinematographic material (6) presented uninterrupted during blood oxygenation level-dependent functional MRI (BOLD-fMRI). In experiment 1, participants (80 healthy volunteers) also saw a neutral movie matched for audiovisual characteristics (table S1) in a separate counterbalanced session. Physiological and psychological stress measures were obtained around and during scanning. Exposure to the aversive movie triggered elevated salivary cortisol ($F(1, 79) = 4.93$, $P = .029$, $P\eta^2 = .06$), salivary alpha amylase (marker of (nor)adrenergic activity; $F(1, 79) = 5.61$, $P = .02$, $P\eta^2 = .07$), heart rate ($F(1, 78) = 44.20$, $P < .001$, $P\eta^2 = .36$), and subjective negative affect ($F(1, 79) = 23.37$, $P < .001$, $P\eta^2 = .23$).

We first identified brain regions that responded preferentially to the aversive movie. Instead of using a pre-specified model that imposes restrictions on the temporal shape of the response that can be detected, we capitalized on the fact that regional activation can be inferred from temporal correlations across subjects (Fig. S1; 13). We observed strong intersubject correlations (ISC) mainly, but not exclusively, in sensory regions for both movies (Fig. 1A&B and Table S2). A contrast between both conditions' ISC maps using non-parametric permutation tests ($P < .05$, whole-brain FWE corrected; 14) revealed relatively little ISC differences in early visual regions. However, we found increased ISC for the aversive movie in regions (Table S3 and Fig. 1C) shown to respond consistently to salient stimuli in meta-analyses of conventional model-based fMRI studies (15, 16). Among these are regions associated with interoception and autonomic-neuroendocrine control (frontoinsular cortex, dorsal ACC, medial PFC, and amygdala; 17-19), peripheral stress effector systems and catecholaminergic signaling (midbrain and hypothalamic regions; 8, 15), and sensory and attentional (re)orienting (thalamus, and inferotemporal and temporoparietal regions; 20). Notably, a similar set of regions forms an intrinsic connectivity network (ICN) in the resting brain that has been proposed to process salience by integrating affective-homeostatic with sensory-attentional information (21). The temporal correlations across subjects found here, however, provide no information about functional connectivity,because different regions may respond to different aspects of the movie and therefore display uncorrelated time courses.

To test for functional connectivity, we used multi-session tensorial probabilistic independent component analysis (ICA). We decomposed fMRI data into time courses, spatial maps, and subject modes, which represent signal variation of each independent component (IC) over time, space, and participants, respectively (see supporting online material; 22). ICA for the aversive condition yielded 18 IC maps (Fig. S2), which represent spatially dissociable signal fluctuations originating from separable large-scale neural ensembles (or nuisance sources). Using objective template matching (Table S5), we subsequently identified the IC map with the strongest overlap with the ISC contrast map (aversive > control; Fig. 2 and S3). The thereby selected IC map for the aversive condition contained all regions mentioned in the previous paragraph except medial PFC (see Fig. 2 and Table S4 for all coactivated

regions). Furthermore, template matching onto a map of the aforementioned salience processing ICN, kindly provided by the authors (21), yielded the same IC map (Table S5). In the remainder, we therefore refer to the selected IC map as the salience network (21). Notably, the medial PFC appears in another IC map alongside the posterior cingulate cortex, suggesting that these regions form part of another neural system (default mode network; 12).

To investigate whether functional connectivity strength within the salience network was associated with stress measures, we used compound measures resulting from ICA decomposition (22). Network strength correlated positively with cortisol ($\rho(78) = .23$, $P = .037$), alpha amylase ($\rho(78) = .28$, $P = .012$), and negative affect change ($\rho(78) = .25$, $P = .026$), but not heart rate change ($\rho(78) = -.06$, n.s.).

Our findings agree with theories that postulate a dual architecture of cortical attentional control networks. In addition to a dorsal frontoparietal network involved in regulating attention in focal tasks (23), these theories implicate a ventral attention network that differs little in topology from the network identified here in reorienting attention away from focal tasks (20) and maintenance of tonic alertness (24). Spontaneous activity in this network has moreover been associated with electroencephalographic signatures of alertness (25).

A pivotal question following from these observations is to what extent stress-related neuromodulators such as noradrenaline and cortisol drive this network reorganization. To address this, we performed a pharmacological experiment implementing a three-armed double-blind between-subjects design. Sixty participants received either propranolol (40 mg), a β-adrenergic receptor blocker, metyrapone (twice 750 mg), a cortisol synthesis blocker, or placebo (Fig. 3). Stress induction procedures were extended with threat of mild electrical shock to increase effectiveness in raising cortisol but were otherwise identical to experiment 1 (see supporting online material).

We observed robust cortisol responses to stress after placebo ($F(1, 19) = 8.67$, $P = .008$, $P\eta^2 = .31$) and propranolol ($F(1, 19) = 11.93$, $P = .003$, $P\eta^2 = .39$), but not after metyrapone ($F < 1$). Metyrapone lowered cortisol throughout testing ($F(1, 38) = 11.60$, $P = .002$, $P\eta^2 = .23$). Conversely, propranolol selectively lowered alpha amylase throughout testing ($F(1, 37) = 9.10$, $P = .005$, $P\eta^2 = .20$; metyrapone

effect: $F < 1$), and lowered heart rate ($F(1, 35) = 29.11$, $P < .001$, $P\eta^2 = .45$; metyrapone effect: $F(1, 36) = 1.7$, n.s.). Neither drug affected subjective negative affect ($F < 1$). Thus, as intended, propranolol and metyrapone selectively affected (peripheral) noradrenergic and glucocorticoid measures, respectively (Fig. 3).

ICA (Fig. S4) and template matching of IC maps between experiments 1 and 2 closely reproduced the salience network IC map (Fig. 4A and table S5). We investigated drug effects on functional connectivity strength within this network in comparison with a visual network as control for specificity. A 3 (drug) * 2 (IC) ANOVA yielded a drug by IC interaction ($F(2, 57) = 3.46$, $P = .038$, $P\eta^2 = .11$). Further testing revealed a drug main effect on the salience ($F(2, 57) = 3.19$, $P = .049$, $P\eta^2 = .10$) but not the visual ($F < 1$, n.s.) network. A planned contrast showed that this effect was carried by a reduction in the propranolol group compared to the other groups ($F(1, 57) = 5.61$, $P = .021$, $P\eta^2 = .09$). Finally, directed one-tailed t-tests demonstrated that propranolol reduced network strength relative to both placebo ($t(38) = 1.64$, $P = .054$) and metyrapone ($t(38) = 2.41$, $P = .011$) groups.

This finding concurs with theoretical frameworks of LC function, which ascribe attentional reorienting functions to cortical noradrenergic projections that parallel those proposed for cortical components of the salience network (20). Animal studies have shown that LC neurons exhibit two distinct functional modes for regulating sensory gain (26). In mildly aroused states optimal for focal task performance, the LC responds phasically to task-relevant stimuli (9), engaging alpha-2A receptors that strengthen top-down dorsolateral PFC regulation of attention (*7*). Under stress, however, LC neurons shift to tonically elevated firing rates associated with distractibility and hypervigilance (10). High tonic firing releases large concentrations of norepinephrine, which engages lower-affinity beta-adrenergic receptors that impair top-down attentional control, but enhance thalamic and sensory functions (*7*). Thus, besides effects on memory (3, 4), a putative function of these neuromodulatory signals is to send interrupt signals to active functional networks (27), causing disengagement from current task sets (9) and promoting fast adaptation by rearranging network activity (11). Our findings establish a causal link between stress-induced noradrenergic activity and activation of the salience network (20).

Although functional connectivity within the salience network correlated with cortisol increases (experiment 1), our finding that cortisol blockade had no effect suggests that cortisol elevation is not necessary for this network reorganization to occur. It has been suggested that corticosteroids act through mineralocorticoid receptors to promote vigilance in immediate response to stress (1). However, recent studies show that exogenous cortisol reduces phobic fear (28) and amygdala responsiveness (29), pointing towards a role for cortisol in preventing overshoot and down-regulation of stress responses. Nonetheless, we cannot exclude the possibility that with different timing or stronger elevations of cortisol interactive or additive effects may occur (4).

In conclusion, we show that noradrenergic neuromodulatory activity in the early phase of the stress response drives a reallocation of neural resources towards a distributed network of regions involved in attentional reorienting, vigilant perceptual intake, and autonomic-neuroendocrine control.

References and Notes

1. E. R. De Kloet, M. Joels, F. Holsboer, Stress and the brain: from adaptation to disease. Nat. Rev. Neurosci. 6, 463 (2005).

2. H. J. F. van Marle, E. J. Hermans, S. Qin, G. Fernández, From specificity to sensitivity: how acute stress affects amygdala processing of biologically salient stimuli. Biol. Psychiatry 66, 649 (2009).

3. L. Cahill, B. Prins, M. Weber, J. L. McGaugh, Beta-adrenergic activation and memory for emotional events. Nature 371, 702 (1994).

4. B. Roozendaal, B. Mcewen, S. Chattarji, Stress, memory and the amygdala. Nat. Rev. Neurosci. 10, 423 (2009).

5. M. Joëls, Z. Pu, O. Wiegert, M. S. Oitzl, H. J. Krugers, Learning under stress: how does it work? Trends. Cogn. Sci. 10, 152 (2006).

6. S. Qin, E. J. Hermans, H. J. van Marle, J. Luo, G. Fernández, Acute psychological stress reduces working memory-related activity in the dorsolateral prefrontal cortex. Biol. Psychiatry 66, 25 (2009).

7. A. F. Arnsten, Stress signalling pathways that impair prefrontal cortex structure and function. Nat. Rev. Neurosci. 10, 410 (2009).

8. Y. M. Ulrich-Lai, J. P. Herman, Neural regulation of endocrine and autonomic stress responses. Nat. Rev. Neurosci. 10, 397 (2009).

9. G. Aston-Jones, J. D. Cohen, An integrative theory of locus coeruleus-norepinephrine function: adaptive gain and optimal performance. Annu. Rev. Neurosci. 28, 403 (2005).

10. R. J. Valentino, E. Van Bockstaele, Convergent regulation of locus coeruleus activity as an adaptive response to stress. Eur. J. Pharmacol. 583, 194 (2008).

11. S. Sara, The locus coeruleus and noradrenergic modulation of cognition. Nat. Rev. Neurosci. 10, 211 (2009).

12. M. D. Fox, M. E. Raichle, Spontaneous fluctuations in brain activity observed with functional magnetic resonance imaging. Nat. Rev. Neurosci. 8, 700 (2007).

13. U. Hasson, Y. Nir, I. Levy, G. Fuhrmann, R. Malach, Intersubject synchronization of cortical activity during natural vision. Science 303, 1634 (2004).

14. M. T. R. van Kesteren, G. Fernández, D. G. Norris, E. J. Hermans, Persistent schema-dependent hippocampal-neocortical connectivity during memory encoding and postencoding rest in humans. Proc Natl Acad Sci USA 107, 7550 (2010).

15. H. Kober et al., Functional grouping and cortical-subcortical interactions in emotion: a meta-analysis of neuroimaging studies. Neuroimage 42, 998 (2008).

16. S. Smith et al., Correspondence of the brain's functional architecture during activation and rest. Proc. Natl. Acad. Sci. U. S. A. 106, 13040 (2009).

17. H. D. Critchley, Neural mechanisms of autonomic, affective, and cognitive integration. J. Comp. Neurol. 493, 154 (2005).

18. J. C. Pruessner et al., Deactivation of the limbic system during acute psychosocial stress: evidence from positron emission tomography and functional magnetic resonance imaging studies. Biol. Psychiatry 63, 234 (2008).

19. T. D. Wager et al., Brain mediators of cardiovascular responses to social threat: part I: Reciprocal dorsal and ventral sub-regions of the medial prefrontal cortex and heart-rate reactivity. Neuroimage 47, 821 (2009).

20. M. Corbetta, G. Patel, G. Shulman, The Reorienting System of the Human Brain: From Environment to Theory of Mind. Neuron 58, 306 (2008).

21. W. W. Seeley et al., Dissociable intrinsic connectivity networks for salience processing and executive control. J. Neurosci. 27, 2349 (2007).

22. C. F. Beckmann, S. M. Smith, Tensorial extensions of independent component analysis for multisubject FMRI analysis. Neuroimage 25, 294 (2005).

23. J. L. Vincent, I. Kahn, A. Z. Snyder, M. E. Raichle, R. L. Buckner, Evidence for a frontoparietal control system revealed by intrinsic functional connectivity. J. Neurophysiol. 100, 3328 (2008).

24. N. U. F. Dosenbach, D. A. Fair, A. L. Cohen, B. L. Schlaggar, S. E. Petersen, A dual-networks architecture of top-down control. Trends. Cogn. Sci. 12, 99 (2008).

25. S. Sadaghiani et al., Intrinsic connectivity networks, alpha oscillations, and tonic alertness: a simultaneous electroencephalography/functional magnetic resonance imaging study. J. Neurosci. 30, 10243 (2010).

26. C. W. Berridge, B. D. Waterhouse, The locus coeruleus-noradrenergic system: modulation of behavioral state and state-dependent cognitive processes. Brain Res. Rev. 42, 33 (2003).

27. S. Bouret, S. Sara, Network reset: a simplified overarching theory of locus coeruleus noradrenaline function. Trends Neurosci. 28, 574 (2005).

28. L. M. Soravia et al., Glucocorticoids reduce phobic fear in humans. Proc. Natl. Acad. Sci. U. S. A. 103, 5585 (2006).

29. M. J. A. G. Henckens, G. A. Van Wingen, M. Joels, G. Fernandez, Time-Dependent Effects of Corticosteroids on Human Amygdala Processing. J. Neurosci. 30, 12725 (2010).

30. Erno Hermans (451.07.019) and Guillén Fernández (918.66.613) received grants from the Netherlands Organisation for Scientific Research (NWO). We thank William Seeley, Vinod Menon, Christian Beckmann, and Elizabeth Phelps.

Supporting Online Material

www.sciencemag.org

Materials and Methods

Tables S1 to S5

Figs. S1 to S4

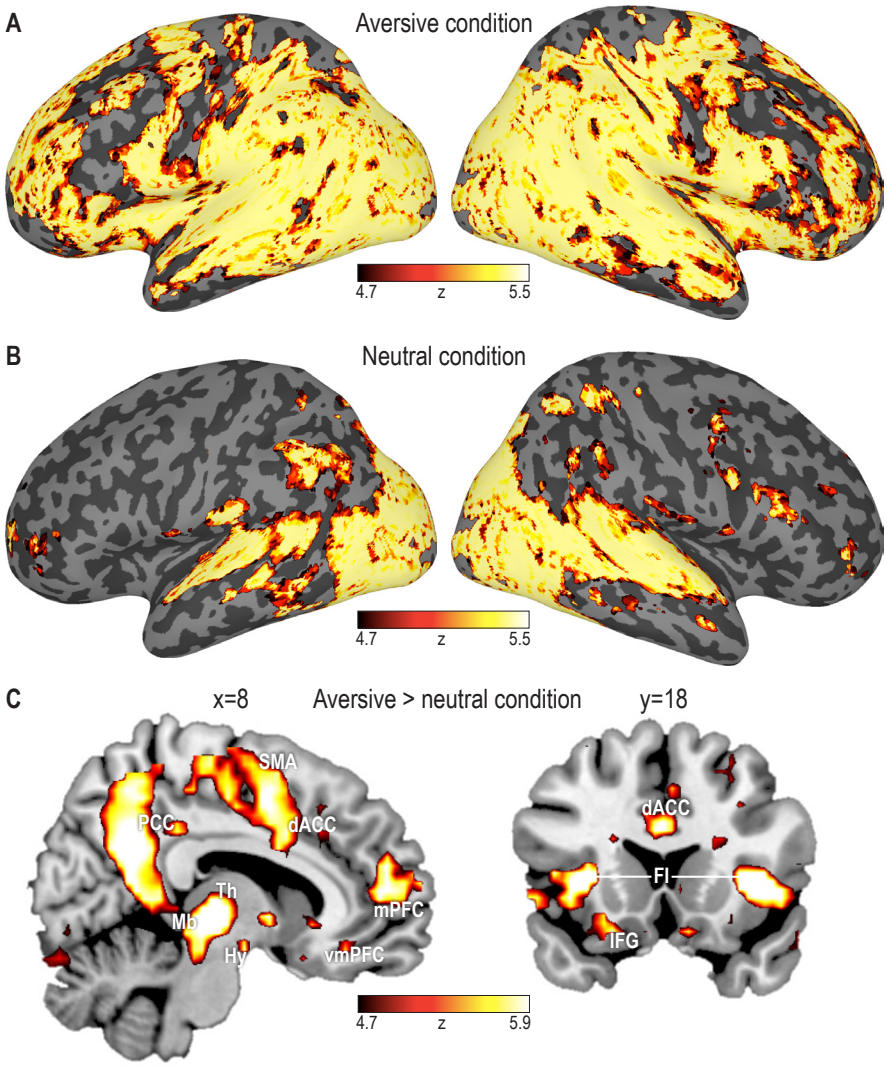

Fig. 1: Intersubject correlations. Maps are thresholded at P < .05, whole-brain FWE corrected, and overlaid onto cortical surface renderings (A&B) and a T1-weighted MRI (C). FI, frontoinsular cortex; dACC, dorsal anterior cingulate cortex; SMA; supplementary motor area; PCC, posterior cingulate cortex; (v)mPFC, (ventro)medial prefrontal cortex; IFG, inferior frontal gyrus; Th, thalamus; Mb, midbrain; Hy, hypothalamus.

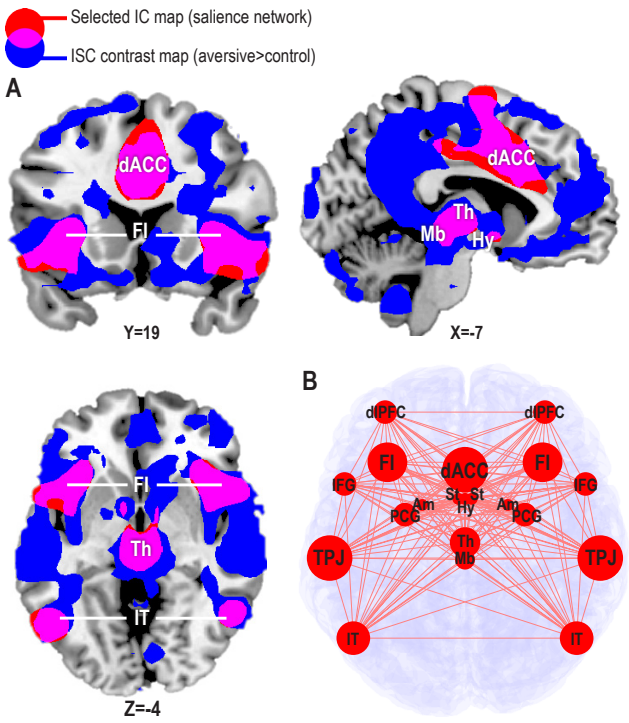

Fig. 2: Regions comprising the selected IC map (salience network; red). A: Overlap (pink) with ISC contrast map (blue; $P < .001$). B: Schematic overview of suprathreshold clusters and relative sizes. FI, frontoinsular cortex; dACC, dorsal anterior cingulate cortex; Mb, midbrain; Hy, hypothalamus; Th, thalamus; IT, inferotemporal cortex; TPJ, temporoparietal junction; Am, amygdala; IFG, inferior frontal gyrus; PCG, precentral gyrus; dlPFC, dorsolateral prefrontal cortex; St, striatum (caudate/pallidum).

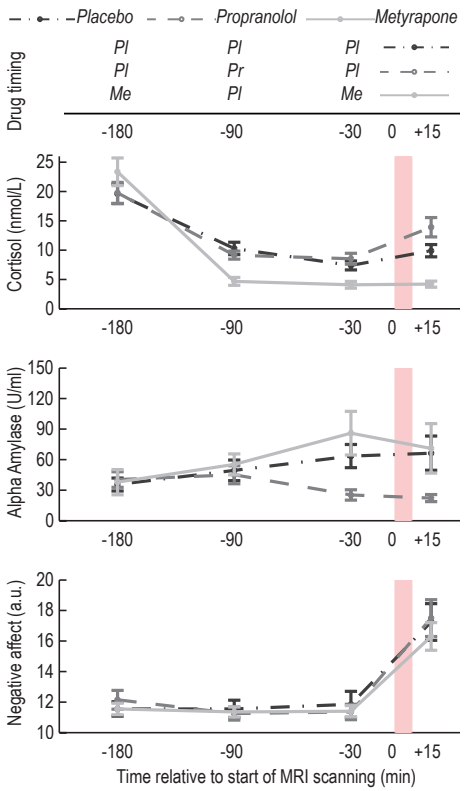

Fig. 3: Timing and effects (+-SEM) of drug administration. Shaded red bars indicate stressor (average time: 12:30 p.m.). Pl, placebo; Pr, propranolol; Me, metyrapone.

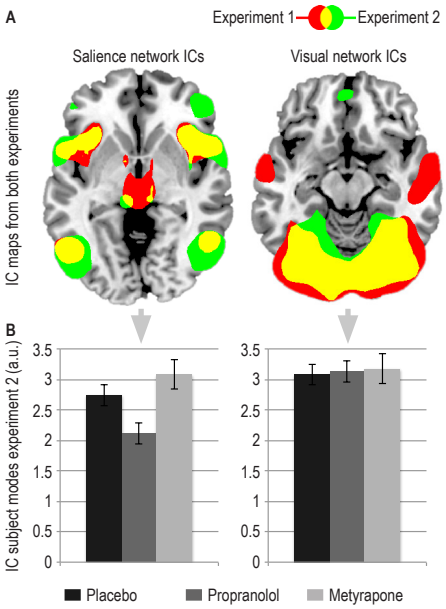

Fig. 4: Drug effects on functional connectivity within salience and visual (control) network ICs. A: Overlap between the IC maps from both experiments ($P < .001$). B: Functional connectivity strength (+-SEM) within both ICs for drug conditions (experiment 2).

Supporting Online Material for

Stress-related Noradrenergic Activity Prompts Large-scale Neural Network Reconfiguration

Erno J. Hermans, Hein J.F. van Marle, Lindsey Ossewaarde, Marloes J.A.G. Henckens, Shaozheng Qin, Marlieke T.R. van Kesteren, Vincent C. Schoots, Helena Cousijn, Mark Rijpkema, Robert Oostenveld, & Guillén Fernández

correspondence to: erno.hermans@donders.ru.nl

This PDF file includes:

Materials and Methods

Participants

For experiment 1 and 2, participants were 80 healthy adult volunteers (53 males, age range 18-38; mean 22.5) and 60 healthy adult male volunteers (age range 18-37; mean 22.7), respectively. Exclusion criteria for both experiments were: current or lifetime history of psychiatric, neurological, or endocrine illness, body mass index outside 18.5-30 range, abnormal hearing or (uncorrected) vision, average use of more than 3 alcoholic beverages daily, current treatment with any medication that affects central nervous system or endocrine systems, average use of recreational drugs weekly or more, habitual smoking, use of antidepressants or corticosteroids, predominant left-handedness, irregular sleep/wake rhythm, intense daily physical exercise, current stressful experience or major life event, current parodontitis, regular exposure to extremely violent movies or computer games. Additionally, participants needed to be free of contraindications for MRI (presence of metal objects in or around the body, claustrophobia). Additional exclusion criteria for experiment 2 were contraindications for propranolol (history of cardiac disease, obstructive respiratory disease, chronic renal failure, hyperthyroidism, diabetes mellitus, Raynaud's syndrome, A-V block, sinus bradycardia [heart rate <60 BPM], and hypotension [SBP < 90mmHg or DBP < 60mmHg]) and for metyrapone (plasma cortisol below 150 or above 700 nmol/l). Women were excluded from experiment 2 to avoid confounds related to menstrual cycle or oral contraceptive use (see S1). A separate sample of 16 volunteers (8 males, aged 20-33) provided subjective ratings of the movie clips.

For 72 hrs prior to each experimental session (in both experiments), all participants were required to maintain a regular sleep-wake cycle and to use no recreational drugs. For 24 hrs prior to testing, they were instructed to refrain from drinking alcohol, intense physical exercise, and smoking. Additionally, they were instructed to not to brush their teeth, floss, eat, and drink anything but water for two hours prior to testing.

All procedures were approved by the local ethical review board (CMO region Arnhem-Nijmegen) in accordance with the declaration of Helsinki and all participants provided written informed consent. Participants received financial reimbursement.

Design and Procedures experiment 1

Participants were tested in a crossover design with stress induction (aversive vs. neutral control movie clip) as within subject factor. Order of test sessions was counterbalanced. All participants underwent fMRI twice, with at least two hours between the two separate sessions. All MRI scans were acquired between 1 p.m. and 10 p.m. because cortisol levels during this period are less variable than during mornings.

Participants arrived in the laboratory at least 1.5 hours prior to scanning and completed the trait scale of Spielberger's State-Trait Anxiety Inventory (STAI; S2), Beck's Depression Inventory (S3), and the Positive and Negative Affect Schedule (PANAS) questionnaire (S4). From all participants, saliva samples were obtained using Salivette collection devices approximately -20 min and +15 min relative to the start of

MRI scanning. During MRI scan sessions, participants were exposed to uninterrupted presentation of either the aversive or the neutral movie clip (see description below). The +15 min sample was taken in the scanner while participants again completed the PANAS questionnaire. Participants performed cognitive tasks in the scanner after exposure to the movie clip (reported in S5-S7).

Design and Procedures experiment 2

Participants in experiment 2 were tested in a randomized, double-blind, placebo-controlled between-subjects design with drug (propranolol, metyrapone, or placebo) as between subjects factor. Experiment 2 consisted of only a single (stress induction) session. No participants had volunteered in experiment 1. At least one week prior to the actual test session, participants underwent a medical screening during which blood pressure, ECG, and a blood sample was obtained, and participants completed the STAI (S2) and BDI (S3) questionnaires. Non-stress baseline saliva samples were collected (at 12 p.m. and at 6 p.m.) on a different day prior to the MRI test session. Experimental groups did not differ in age, mean non-stress baseline salivary cortisol levels, mean non-stress baseline salivary alpha amylase levels, baseline positive and negative affect (on test days), baseline heart rate (during screening), STAI scores, or BDI scores (all $F < 1$).

Test days started between 7 a.m. and 9 a.m. and participants remained under medical surveillance until leaving the laboratory 11 hours later. Participants were instructed to only drink water before coming to the laboratory but were allowed to eat at controlled time-points during the experimental day. Upon arrival, compliance with instructions was verified. Saliva samples were collected using Salivette collection devices at approximately -180 min, -90 min, -30 min, and +15 min relative to the start of the aversive movie (at the beginning of the MRI scan session). On average, the aversive movie started at 12:30 p.m. (see Fig. 3). This earlier time point (compared to experiment 1) was chosen to ensure higher natural baseline levels of cortisol at the time of testing (due to the diurnal cycle), and thus to maximize the difference in cortisol levels between the metyrapone group and the other two groups. Saliva sampling always coincided with completion of PANAS (S4) questionnaires. Participants received either propranolol, metyrapone, or placebo capsules after saliva sampling.

Propranolol is a non-selective β-adrenergic receptor blocking agent which competes with β-adrenergic receptor stimulating agents at β1- and β2-adrenergic receptor sites. Peak plasma concentrations are reached 1 to 2 hours after administration. In line with previous studies, we therefore administered 40 mg of propranolol orally 90 min prior to scanning (cf. S8). Propranolol has both central and peripheral effects. Peripheral beta-adrenergic blockade at the level of target organs such as the heart may reduce the efficacy of circulating (nor)adrenaline to stimulate ascending projections from the vagus nerve to nucleus of the solitary tract (NTS). Vagal afferents to the NTS stimulate noradrenergic projections directly to the amygdala, but also (both directly and indirectly) to the LC (S9, S10). Consequently, in addition to central β-adrenergic receptor blockade, propranolol may also reduce central availability of NE (but see S11). Peripherally, propranolol moreover causes a sharp decline of salivary alpha amylase (S12) because alpha amylase is stimulated via sympathetic innervation of the salivary glands through beta-adrenergic receptors (S13).

Metyrapone reduces cortisol production by inhibiting the 11-β-hydroxylation reaction in the adrenal cortex (S14). Peak plasma concentrations are usually reached 60 minutes after administration, but metyrapone is rapidly eliminated from plasma. In line with previous studies, we therefore administered 750 mg of metyrapone twice (see S1, S15), at 180 min and 30 min before the start of scanning. In addition, 1 mg of dexamethasone was given at the end of the test day when leaving to restore availability of glucocorticoids and avoid acute adrenal insufficiency. It should be noted that as a consequence of reduced glucocorticoid feedback, hypothalamic CRH/AVP and pituitary release of ACTH into plasma is likely increased after administration of metyrapone, which in turn may have central effects (S16). Metyrapone may also itself exert central effects at the level of the PVN and higher brain areas (S17).

Placebos were capsules containing primojel FNA and were visually indistinguishable from verums. Because metyrapone and propranolol required different timing of administration, it was necessary to administer additional placebos at all drug administration time points to maintain the (double) blinding (see Fig. 3 for timing of drug administration).

During MRI scan sessions, participants watched an uninterrupted presentation of the aversive movie clip (see below). In addition, we extended this stress induction procedure with threat of mild electrical shock to the fingers throughout the presentation of the aversive movie clip. However, no shocks were delivered during movie presentation or between movie presentation and saliva sampling at the +15 time point. The reason for this addition was to assure a more robust cortisol response to the stress induction procedure and thus also to maximize the difference in cortisol levels between the metyrapone group and the other two groups. Following the aversive movie, participants performed a memory task (to be reported elsewhere). During this task, but after the +15 saliva sample (see Fig. 3), they received mild electrical shock twice (2 ms block pulses administered at 50 Hz, 1.75 mA, duration of 100 ms and 200 ms, respectively) through Ag/AgCl electrodes attached to the distal phalanges of the index and middle fingers of the left hand.

Aversive cinematographic material

A primary goal of the present study was to create an optimally ecologically valid model for studying neurocognitive processes elicited by acutely stressful experiences in the real world that may ultimately trigger emotional trauma in a severe form. We chose to use exposure to strongly aversive cinematographic material for the following reasons. Highly aversive films satisfy the requirements for the neuroendocrine stress response in humans as described by Mason (S18): unpredictability, novelty, and uncontrollability. In agreement, previous research from our laboratory and others has shown that aversive cinematographic material can elicit psychological and physiological manifestations of stress (S19-S22). Unlike stressors based on cognitive performance in combination with negative social evaluation (e.g., S23-S25), this type of stressor is likely to yield emotion-focused rather than problem-focused coping strategies (S26) and plausibly triggers a state of fearful arousal. The emotion fear is associated with enhanced attention to salient information in the environment (S27) and is amygdala dependent (S28), making this type

of stressor more closely related to amygdala-dependent stressors used in animal research (e.g., S29).

Fragments (both 140 s) from two different movies entitled "Irréversible" (2002), by Gaspar Noé, and "Comment j'ai tué mon père" (2001), by Anne Fontaine, were selected to serve as aversive and neutral control movie clips, respectively. The neutral movie clip was only used in experiment 1. The aversive film was approved by the NICAM (Dutch Institute for Audiovisual Media) for viewers above 16 years (the highest age category). Matching for audiovisual characteristics (see table S1) was performed by the authors by selecting aversive and neutral clips out of a set of candidate clips which best matched on the following measures: presence of faces in the foreground, presence of background actors, amount of distinct camera movements, and percentage of time the camera was moving. Selected aversive scenes contained extreme male-to-male aggressive behavior and violence in front of a crowd. Neutral control scenes also contained people interacting in the foreground in the presence of a background crowd. Fragments were equalized in luminance. Both movies are French spoken, but selected movie clips contained minimal speech.

To verify whether the aversive movie clip as opposed to the neutral control movie had the intended effects on subjective affect, we obtained subjective ratings of the movie clips from an additional sample of 16 healthy volunteers with counterbalanced viewing order (see table S1). The aversive movie was rated with lower valence and higher arousal scores. For the aversive movie, participants reported less positive affect and control of the situation, and more fear, anger, repulsion, surprise, stress, and anxiety about what was to come in the movie. Participants reported no difference in subjective feelings of shame, sadness, or social evaluation. Finally, subjective ratings of total amount of movement (obtained because it is difficult to quantify all aspects of movement objectively) and viewer engagement did not differ, and plot complexity was rated as slightly higher for the neutral control movie.

Movie clips were back-projected onto a translucent screen. Participants were notified that watching the movie clips could be stressful, and that they could terminate their participation at any time. Participants were moreover instructed to lie as still as possible, keep their eyes open, watch the movie clips for the entire time that it was presented, and to imagine being an eyewitness to the events in the movie. A 50 Hz iView system with MR-compatible MEyeTrack-LR eye-tracking device mounted on the scanner bed was used to ascertain that participants watched the entire movie clip. Cardiac rhythm of the participants was monitored throughout BOLD-fMRI scanning using an infrared pulse oximeter affixed to the left index finger.

MRI scan acquisition

Participants lay in the scanner in a supine position, head movement was restricted using foam padding, and participants wore ear plugs and MR compatible headphones. For experiment 1, MRI scans were collected using a 3.0 Tesla MRI scanner equipped with an 8 channel head coil. The following scans were obtained: 70 (per session) T2* weighted BOLD images (gradient echo EPI, TE/TR: 25/2180 ms, flip angle: 90°, FOV: 212*212 mm, matrix: 64*64, 3 mm slice thickness, .3 mm slice gap, 37 ascending axial slices. Structural scans were obtained using a Magnetization-Prepared RApid Gradient Echo

(MP-RAGE) sequence combined with GeneRalized Autocalibrating Partially Parallel Acquisitions (GRAPPA; S30) with the following parameters: TE/TR: 2.96/2300 ms, flip angle: 8°, FOV: 256*256*192 mm, voxel size: 1 mm isotropic, GRAPPA acceleration factor 2. Data for experiment 2 were acquired using a 1.5 Tesla MRI scanner with 8 channel head coil. Gradient echo EPI (65 volumes) parameters were: TE/TR: 35/2340 ms, flip angle 90°, FOV: 212*212 mm, matrix 64*64, 3.5 mm slice thickness, 0.35 mm slice gap, 32 ascending axial slices. MP-RAGE sequence parameters were: TE/TR: 3.68/2250 ms, flip angle: 15°, FOV: 256*256*176 mm, voxel size: 1 mm isotropic, GRAPPA acceleration factor 2. For EPI images, relatively short TEs and oblique axial angulation were chosen to minimize signal dropout due to magnetic field inhomogeneity around air-tissue interfaces. The first EPI five volumes of each run were discarded to allow for T1 equilibration.

Biochemical analyses of saliva samples

Samples were frozen at -25°C until assayed. Biochemical analysis of salivary cortisol and α-amylase were performed at the Department of Biopsychology, TU Dresden, Germany. Saliva samples were prepared for biochemical analysis by centrifuging at 3,000 rpm for 5 minutes, which resulted in a clear supernatant of low viscosity. Salivary free cortisol concentrations were subsequently measured using a commercially available chemiluminescence immunoassay with high sensitivity of 0.16 ng/ml. Concentration of α-amylase in saliva was measured by an enzyme kinetic method: saliva was processed on a Genesis RSP8/150 liquid handling system. First, saliva was diluted 1:625 with double-distilled water by the liquid handling system. Twenty microliters of diluted saliva and standard were then transferred into standard transparent 96-well microplates. Standard was prepared from "Calibrator f.a.s." solution with concentrations of 326, 163, 81.5, 40.75, 20.38, 10.19, and 5.01 U/l α-amylase, respectively, and bidest water as zero standard. After that, 80 ml of substrate reagent (a-amylase EPS Sys) were pipetted into each well using a multichannel pipette. The microplate containing sample and substrate was then warmed to 371C by incubation in a waterbath for 90 s. Immediately afterwards, a first interference measurement was obtained at a wavelength of 405 nm using a standard ELISA reader. The plate was then incubated for another 5 min at 371C in the waterbath, before a second measurement at 405 nm was taken. Increases in absorbance were calculated for unknowns and standards. Increases of absorbance of diluted samples were transformed to α-amylase concentrations using a linear regression calculated for each microplate.

As a response measure for both experiments, we calculated the area under the curve with respect to increase (AUCi) for both measures (S31) using the last sample prior to, and the sample following, the start of MRI scanning. Note that electrical shocks were not delivered before the final saliva sample was obtained in experiment 2, and that no (threat of) shock was employed in experiment 1.

Analysis of PANAS data

Baseline corrected PANAS scores were calculated by subtracting PANAS scores obtained simultaneously with the last saliva sample before the start of scanning (-20 for

experiment 1, -30 for experiment 2) from the PANAS score obtained with the saliva sample after scanning (at +15).

Analysis of pulse oximeter data

Heart rate infrared pulse oximeter data were carefully inspected for movement-related and other measurement artifacts using in-house developed software before calculation of averaged beats per minute (BPM) values per movie presentation. Three participants (experiment 2) were excluded from pulse oximeter data analyses due to excessive artifacts in the recorded signal, but were included in all other analyses.

Statistical analyses of physiological and psychological measures

For experiment 1, AUCi measures of salivary cortisol and alpha amylase, heart rate (BPM) during the two movie clips, and baseline corrected PANAS scores were entered into repeated measures ANOVAs controlling for order of testing. Correlations of these stress measures with fMRI data were performed using non-parametric Spearman's rank order tests. For experiment 2, repeated measures ANOVAs were additionally used to characterize drug effects across multiple measurements throughout the day. Alpha was set at .05 throughout. Partial η squared ($P\eta^2$) effect size estimates are reported for all ANOVAs.

Functional MRI pre-processing

MR scans were spatially pre-processed using SPM5 (http://www.fil.ion.ucl.ac.uk/spm; Wellcome Department of Imaging Neuroscience, London, UK). Motion correction was performed on all functional scans using a rigid body transformation and sum of squared differences minimization. All participants remained within 3 mm movement in both sessions. Additionally, we calculated the average amount of scan-to-scan three-dimensional movement for the stress and neural sessions (cf. S32) to determine whether there were differences in movement between the two sessions. This calculation revealed no significant difference in mean scan-to-scan translations between the aversive movie (.074 mm/scan) and the neutral control condition (.083 mm/scan): $t(79) = 1.02$, n.s.). In experiment 2, no differences were found in movement between groups (mean .045 mm/scan; drug effect: $F < 1$).

Mutual information maximization based rigid body registration was employed to register functional and individual structural scans. Subsequently, all images were normalized to standard (MNI152) space using affine transformations and non-linear deformations, and resampled into 3.5 mm isotropic voxels using 4th degree B-spline interpolation. Finally, all images were smoothed using an 8 mm FWHM Gaussian kernel to accommodate residual between subjects variance in (functional) anatomy. Resulting images were subjected to ISC analysis and independent component analysis as described below.

ISC analysis

ISC analysis (used for experiment 1) was implemented using custom scripts combined with cluster-based nonparametric randomization tests as implemented in the Matlab toolbox FieldTrip (http://www.ru.nl/neuroimaging/fieldtrip; Donders Centre for Cognitive Neuroimaging, Nijmegen, The Netherlands), a Matlab toolbox for the analysis of biological data (S33).

First, low frequency confounds (.01 Hz cut-off discrete cosine transform high pass filter) and movement-correlated (six parameter rigid body transformation-derived translations and rotations) signals were removed from all subjects' functional scans series through residualization. Second, data were masked using a MNI152 space grey matter tissue probability map (see International Consortium for Brain Mapping: http://www.loni.ucla.edu/ICBM/Downloads/Downloads_ICBMprobabilistic.shtml) with a probability threshold of .45, allowing for extraction of the global grey matter signal (c.f. S34), i.e., the mean BOLD signal time course over all grey matter voxels of a single participant. Third, this global grey matter signal was also regressed out of each voxels' time course, resulting in filtered 3D time course data for each participant. This procedure partials out any variance explained by global grey matter BOLD signal fluctuations and therefore enhances the regional specificity of the ISC effects.

Statistical analysis was performed using cluster based nonparametric randomization tests (see S35, S36) as implemented in FieldTrip and using custom mass univariate statistical functions sensitive to the effects of interest. Two different such functions were devised: 1) ISC main effect, testing regional ISC within a single session per subject dataset, and 2) pairwise comparison of ISC within a dataset with two sessions per subject.

First, ISC main effects were calculated as follows (see fig. S1 for an example): for each voxel, each subject's time course was correlated with the mean of all other subjects' time courses in the same voxel, and this correlation was expressed in a t-statistic, thus resulting in one ISC map for each participant. Subsequently, a one-sample t-test was run across these subject-specific ISC maps. To accommodate dependencies within these t-statistics, non-parametric randomization tests were applied to validly test the null hypothesis of zero ISC across the group. Specifically, this procedure tests the null hypothesis (H0) that the time course data of a random set of subjects can be sign permuted without affecting the ISC t-statistic across the group. This map-wise sign permutation procedure destroys any correlations of time course across subjects without affecting the temporal autocorrelational structure of the signal, the spatial dependencies of the signal, or the dependencies between the subject-specific ISC maps, and can therefore be used to estimate a null distribution. To achieve an accurate approximation of this null distribution, 1,000 randomizations (limited by computational resources) were performed, and the null distribution was pooled across voxels. Subsequently, each voxel's ISC probability under H0 was derived from the proportion of the null distribution exceeding that voxel's value, and expressed in a z-statistic. Voxel-level inferences were based on these z values after applying a (conservative) Bonferroni correction for all tests performed within the whole-brain search region (e.g., alpha = .05 / 41128 voxels; $z > 4.71$, for a whole-brain correction). A more sensitive cluster-based method was also implemented that was based on a randomization-derived null distribution of cluster weights (i.e., the sum of all t-values within a suprathreshold cluster). This null

distribution was obtained by setting a more liberal initial threshold, calculating the cluster weights for each cluster of adjacent suprathreshold voxels, and selecting the largest of these for every randomization. Clusters within the non-randomized ISC map exceeding a threshold based on the 5% largest clusters within all randomizations were considered significant. This method implements an alpha = .05, one-sided, test for cluster significance corrected for multiple comparisons.

Second, pairwise comparisons for the difference in ISC between two sessions, here used to compare ISC for the two different movie conditions, were implemented as follows. Two ISC maps per subject were created, one for each of the two sessions. Then, a voxel-wise paired-samples t-test was performed on these pairs of ISC maps testing for stronger ISC in one condition than the other. We now tested the H0 of exchangeability of conditions. Specifically, the assignments of individual ISC maps to conditions of a random set of participants was randomized 10,000 times (more randomizations were used because this procedure requires less computation) and paired t-test calculations were repeated to generate the null-distribution. Further procedures were identical to the main effect tests.

All statistical parametric maps resulting from ISC analyses were treated as exploratory whole-brain analyses. Because the strong (differential) ISC effects found in these analyses resulted in single clusters covering widespread regions, cluster-based statistical tests could not be used to localize regional peaks of (differential) ISC. Therefore, voxel-wise tests with conservative Bonferroni FWE corrections were used for localization according to the Automatic Anatomical Labeling template (see tables S2 and S3; S37).

For visualization, ISC main effect z-maps of both conditions were rendered onto inflated spatial representations of the cortical surfaces of the left and right hemispheres (figs. 1A and 1B) using an SPM5 surface rendering toolbox (http://spmsurfrend.sourceforge.net) and NeuroLens (http://www.neurolens.org). Results from the ISC contrast analysis (aversive > neutral) are shown in figures 1C and 2, where thresholded ISC z-maps are overlaid onto T1-weighted MR image slices. Left hemispheres are shown on the left, and all slice coordinates are defined in MNI152 space.

Tensorial independent component analysis

Independent component analyses were performed using the FMRIB Software Library's Multivariate Exploratory Linear Optimized Decomposition into Independent Components (FSL-MELODIC; http://www.fmrib.ox.ac.uk/fsl). Specifically, we performed a multi-session tensorial probabilistic independent component analysis (S38). This procedure entails concatenation of individual datasets into a 3D array (time * voxel * subjects) and subsequent decomposition resulting in time courses, spatial maps, and subject modes for each component. These represent the signal variation per component over time, space, and participants, respectively. Such decomposition is known to isolate unidentified, but spatiotemporally structured, sources of nuisance signal (S39), but in addition, may be used to identify and separate neural ensembles involved in task execution (S40) as well as intrinsic connectivity networks (ICN), which exhibit spatiotemporally coherent patterns of spontaneous activity in the absence of a goal-directed task (S41).

Group level (tensorial) independent component analysis of functional MRI data typically yields a large number of independent components (ICs), which reflect various sources that are not of interest, or may be driven by single participants. Therefore, objective selection criteria are needed to select an IC that reflects common activity within a certain connectivity network of interest. We employed an automated template matching procedure comparable to the one used in (S42), with the difference that we did not impose restrictions on the power spectrum of the selected IC because the power spectrum of extrinsically driven network activity may differ from that of intrinsic fluctuations. Moreover, we performed the IC matching procedure directly on the tensorial ICA group maps. First, we calculated for every IC map a goodness-of-fit score by subtracting the mean z-score (z scores could be both positive and negative) of all gray matter voxels outside of the template from the mean z-score of all gray matter voxels inside the template, and selected the component with the highest goodness-of-fit score. Second, the distribution of the subject modes (i.e., a measure of the IC's functional connectivity strength per participant) of selected components was investigated for normality (using the Kolmogorov-Smirnov test) to identify and discard components driven by single subjects, components were tested for an overall effect across the group (using one-sample t-tests; see table S5), and we verified whether selected IC maps comprised our main regions of interest (based on the results of the ISC contrast analysis).

For experiment 1, we used this procedure to select the IC map with the largest spatial overlap with the contrast map for differential ISC between the two experimental conditions (see fig. S3 for the best and second best fits). Additionally, we repeated the template matching procedure for a previously published ICN map template (S43), which was kindly provided by Seeley and colleagues, to ascertain that matching onto this template would yield the same IC map. Subject modes of the selected IC were subsequently used for correlational analyses with stress response measures (AUC of the salivary cortisol response, AUC of alpha amylase change, heart rate change, and change in subjective negative affect) using non-parametric Spearman's rank order correlation tests.

For experiment 2, we used the same procedure to identify the IC corresponding with the IC selected in experiment 1. Moreover, we verified if the two spatially matching IC's also matched in the temporal domain by calculating the correlation between the two time courses (after correcting for differences in sample rate using interpolation). Subject modes of the selected IC and of an occipital control IC comprising early visual regions were subjected to repeated measures ANOVAs to test for drug effects. Further directed tests using AVOVA contrasts and one-tailed t-tests were performed to test a priori hypotheses of a specific effect in the propranolol group on the selected frontoinsular IC. Alpha was set at .05 and effect size estimates ($P\eta^2$) are reported for all relevant tests.

For visualization, independent component maps were thresholded and overlaid onto a T1 weighted canonical image in MNI152 space (figs. 2 and 4, and figs. S2, S3, and S4). Fig. 2B shows a schematic overview of all the regions that correlate with the IC identified as belonging to the salience network. Node locations correspond to anatomical locations viewed from above (anterior-posterior axis is represented from top to bottom). The sizes of nodes moreover approximate cluster sizes. Suprathreshold clusters within selected IC maps are summarized in table S4.

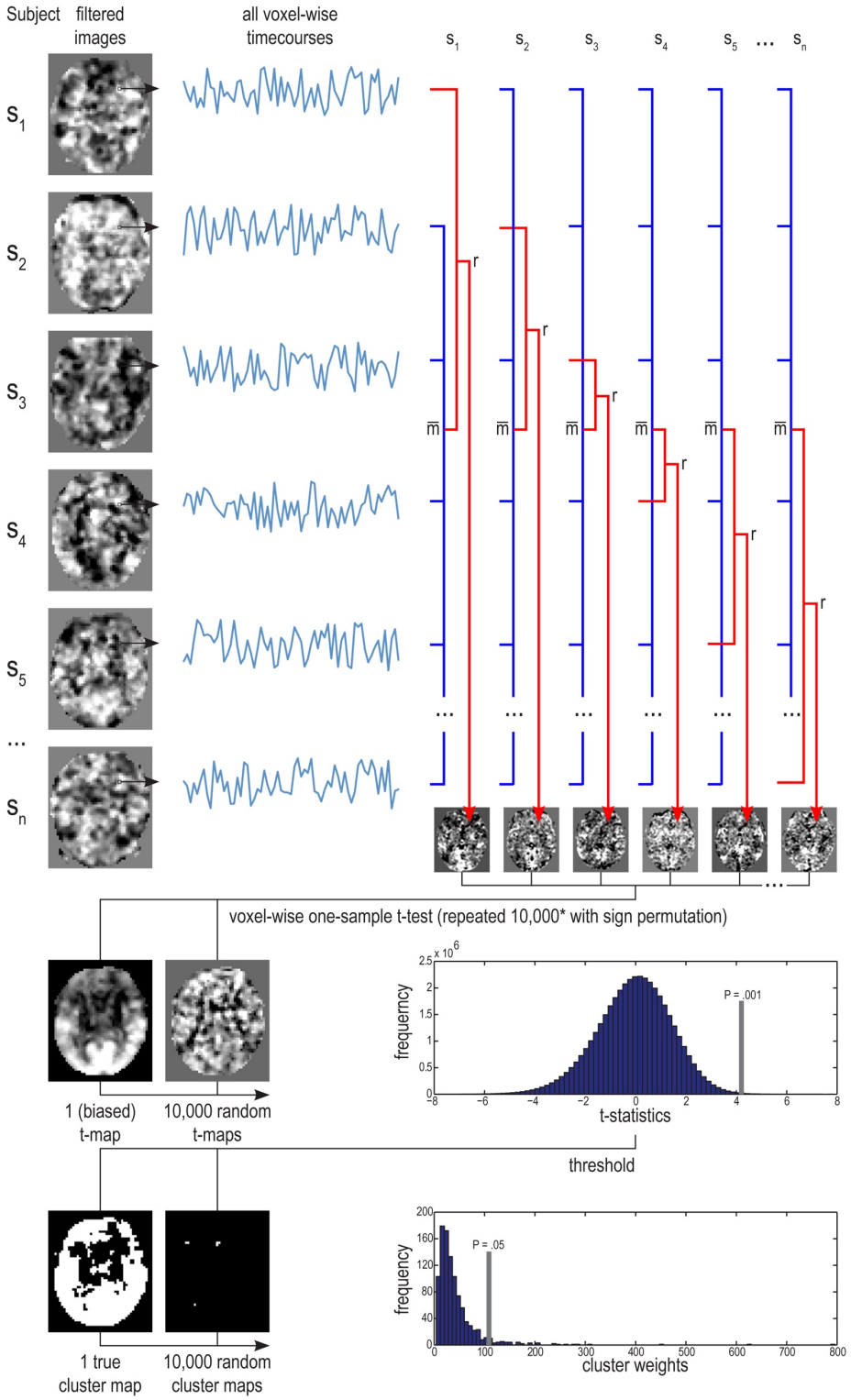

Fig. S1. Chart illustrating the data flow of group level ISC main effect analysis. ISC analysis starts from spatially pre-processed and temporally filtered data ("filtered images"). In the first stage of the analysis, all voxels' time series of a random subset of participants are sign permuted. Then, for every participant, each voxel's time series is

correlated with the mean of all other participants' time series in the same voxel. This procedure results in one ISC map for each participant, for each randomization. Subsequently, these maps are subjected to one-sample t-tests testing the null hypothesis of mean zero correlation across the group, resulting in one t-statistic map representing the group ISC effect and 1000 similar maps resulting from the sign permutations. In the second stage, all t-values from the random t-maps are pooled and used to generate a null distribution. This null distribution is subsequently used to obtain unbiased voxel-level probabilities (which can be expressed as z-statistic) of the biased t-statistic map by determining, for each observed biased t-value, the proportion of t values within the null distribution that exceed this value. In the third and final stage, a (liberal) threshold is applied to obtain the weight (sum of suprathreshold t-values) of the highest-weight cluster of adjacent suprathreshold voxels in each of the 1000 random t-maps, thus creating a cluster weight null-distribution. Finally, the probability of each suprathreshold cluster in the actual t-map can now be obtained by determining the proportion of maximum cluster weights (resulting from randomization) that exceed the weight of that cluster.

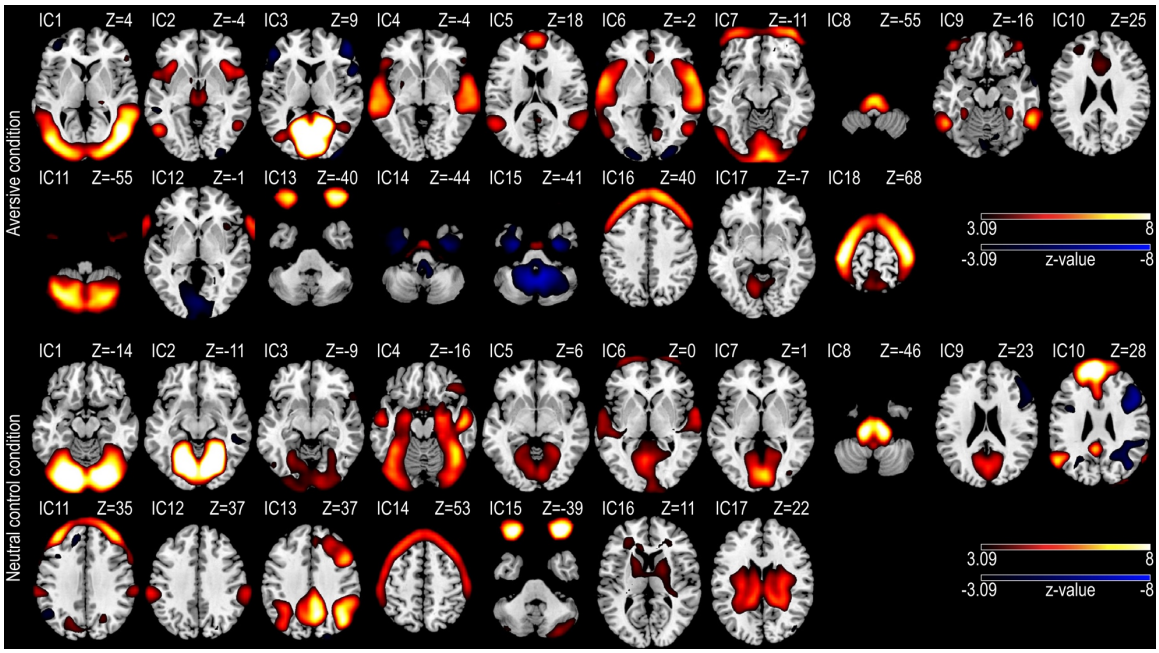

Fig. S2. Overview of spatial maps corresponding with all ICs resulting from tensorial independent component analysis of data recorded during exposure to the aversive movie (18 ICs) and the neutral control movie (17 ICs) from the first experiment. For the aversive movie, template matching procedures (see materials and methods) identified IC2 as the IC with the strongest spatial overlap with both the ISC contrast map (aversive > control) map and the (previously published) ICN template map (S*43*). No match was found for the neutral control movie. For each IC, the axial slice that contains the maximum number of suprathreshold voxels is shown. Statistical maps are thresholded at $Z > 3.09$ ($P < .001$) and overlaid onto a canonical T1-weighted image. Z-coordinates of axial slices are defined in MNI152 space. Left hemispheres are shown on the left. IC, independent component.

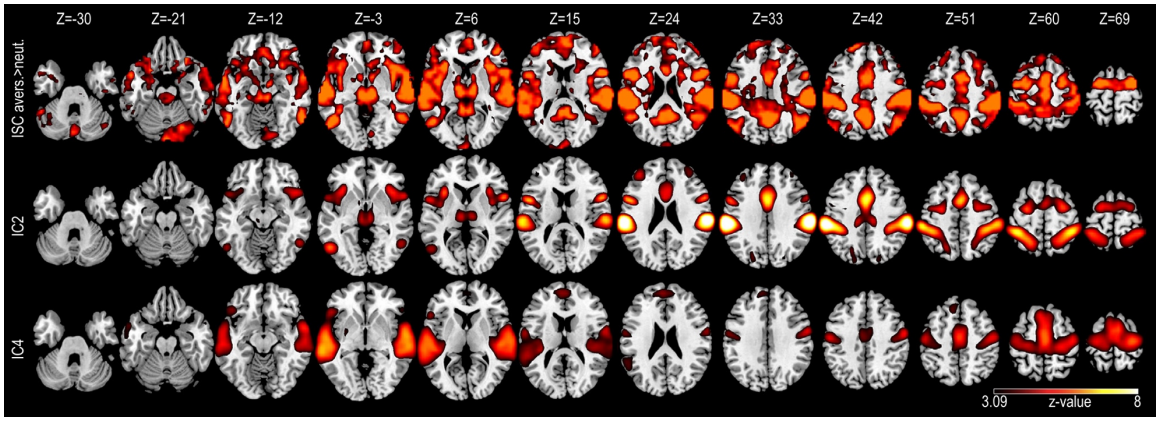

Fig. S3. Results of template matching procedure for experiment 1. The upper panel shows the intersubject correlation difference map between the aversive and neutral conditions (see also figure 1 and supporting online table S3) that was used as template. The middle panel shows the best match among the spatial maps corresponding with the 18 ICs resulting from tensorial independent component analysis of the aversive movie data (IC2; see figure 2 and supporting online table S4). The bottom panel shows the second best fit (IC4, see figure 2). Statistical maps are thresholded at $Z > 3.09$ ($P < .001$) and overlaid onto a canonical T1-weighted image. Z-coordinates of axial slices are defined in MNI152 space. Left hemispheres are shown on the left. ISC, intersubject correlation; avers, aversive movie; neut, neutral control movie; IC, independent component.

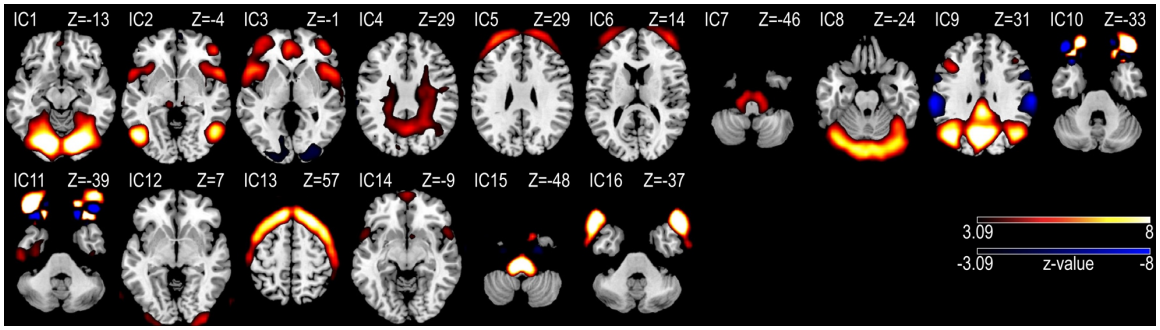

Fig. S4. Overview of spatial maps corresponding with all 16 ICs resulting from tensorial independent component analysis of experiment 2 (data acquired during exposure to the aversive movie clip). For each IC, the axial slice that contains the maximum number of suprathreshold voxels is shown. Statistical maps are thresholded at $Z > 3.09$ ($P < .001$) and overlaid onto a canonical T1-weighted image. Template matching procedures (see materials and methods) identified IC2 as the IC with the strongest spatial overlap with the IC selected for experiment 1. Z-coordinates of axial slices are defined in MNI152 space. Left hemispheres are shown on the left. IC, independent component.

	Aversive movie		Neutral control movie		
	Mean	*SD*	*Mean*	*SD*	*t-value*
Subjective affective ratings:					
Arousal[a]	7.8	1.2	3.9	1.9	9.29***
Valence[a]	1.6	0.9	4.6	1.4	-7.35***
Happiness[b]	4.1	7	29.7	21.4	-4.97***
Fear[b]	60.1	30.9	31.9	30.6	3.63**
Anger[b]	58.9	29.9	9.3	12	6.56***
Repulsion[b]	88.7	17.9	8.9	10.5	15.67***
Surprise[b]	49.3	31	17.4	18.1	3.94**
Shame[b]	16.6	18.1	7.1	8.9	2.03
Sadness[b]	56.6	29.2	43.7	28.8	1.77
Stress[b]	69.6	29.4	31.2	27.2	4.51***
Threat[b]	53.6	28.7	23	26.2	4.21***
Social evaluation[b]	10.2	10.9	9.2	9.8	0.33
Anxiety for events to come[b]	65.1	34.1	42	30.5	3.08*
Lack of control[b]	61.8	31	36.6	27.9	3.33**
Other subjective ratings:					
Plot complexity[b]	14.6	13.9	26.1	19.4	-2.27*
Viewer engagement[b]	44.7	30.4	43.5	27.1	0.16
Amount of movement[b]	52.9	23.1	49.6	24.3	0.42
Objective characteristics:					
Foreground face(s) presence[c]	78%		70%		
Background crowd presence[c]	50%		56%		
Camera moving[c]	71%		85%		
Overt violence[c]	75%		0%		
Distinct camera movements[d]	32		24		

Table S1. Summary of subjective movie ratings and emotional ratings obtained from a separate group of 16 participants and objective characteristics of the aversive and the neutral control movie clips. a, ratings obtained using a self-assessment manikin scale (range 1 - 9); b, ratings obtained using a 0-100 visual analog scale; c, percentage of time; d, number of times; *, $P < .05$; **, $P < .005$; ***, $P < .001$.

Contrast	Left Hemisphere				Right Hemisphere			
Region	x (mm)	y (mm)	z (mm)	Z	x (mm)	y (mm)	z (mm)	Z
Main effect ISC aversive								
Occipital lobe								
superior occipital gyrus	-18	-82	30	>5.44	18	-82	30	>5.44
middle occipital gyrus	-34	-84	13	>5.44	34	-84	13	>5.44
inferior occipital gyrus	-36	-80	-6	>5.44	36	-80	-6	>5.44
cuneus	-5	-78	29	>5.44	5	-78	29	>5.44
calcarine fissure	8	-80	11	>5.44	-8	-80	11	>5.44
lingual gyrus	-20	-63	-3	>5.44	20	-63	-3	>5.44
fusiform gyrus	-30	-54	-14	>5.44	30	-54	-14	>5.44
Temporal lobe								
inferior temporal gyrus	-51	-53	-11	>5.44	51	-53	-11	>5.44
middle temporal gyrus	-55	-34	1	>5.44	55	-34	1	>5.44
superior temporal gyrus	-58	-18	5	>5.44	58	-18	5	>5.44
Heschl gyrus	-44	-21	10	>5.44	44	-21	10	>5.44
Limbic lobe								
temporal pole	-51	12	-28	>5.44	51	12	-28	>5.44
anterior cingulate cortex					0	39	16	>5.44
median cingulate cortex					0	-10	42	>5.44
posterior cingulate cortex					0	-43	29	>5.44
hippocampus	-22	-11	-11	>5.44	22	-11	-11	>5.44
parahippocampal gyrus	-23	-39	-8	>5.44	23	-39	-8	>5.44
Parietal lobe								
superior parietal gyrus	-24	-66	52	>5.44	24	-66	52	>5.44
inferior parietal gyrus	-49	-41	58	>5.44	49	-41	58	>5.44
angular gyrus	-49	-59	32	>5.44	49	-59	32	>5.44
supramarginal gyrus	-54	-34	34	>5.44	54	-34	34	>5.44
precuneus	-8	-57	36	>5.44	8	-57	36	>5.44
Central regions								
precentral gyrus	-35	-5	58	>5.44	35	-5	58	>5.44
postcentral gyrus	-27	-28	62	>5.44	27	-28	62	>5.44
rolandic operculum	-42	-15	18	>5.44	42	-15	18	>5.44
Insular cortex	**-43**	**13**	**-3**	**>5.44**	**43**	**13**	**-3**	**>5.44**
Frontal lobe								
superior frontal gyrus	-21	35	50	>5.44	21	35	50	>5.44
middle frontal gyrus	-45	49	14	>5.44	45	49	14	>5.44
inferior frontal gyrus	-47	25	-2	>5.44	48	47	0	>5.44
paracentral lobule	-5	-27	64	>5.44	5	-27	64	>5.44
supplementary motor area	-5	-3	58	>5.44	5	-3	58	>5.44
gyrus rectus	-3	42	-14	>5.44	3	42	-14	>5.44
olfactory cortex	-17	14	-17	5.25	11	14	-18	5.25
Subcortical regions								
amygdala	-22	-6	-13	>5.44	24	-7	-11	>5.44
caudate nucleus	-9	7	7	5.15	19	12	20	>5.44
putamen	-25	5	3	>5.44	28	3	3	5.37
pallidum	-21	1	0	>5.44	11	6	0	5.41

thalamus	-7	-16	5	>5.44	7	-16	5	>5.44
midbrain	-6	-26	-10	>5.44	6	-26	-10	>5.44
Cerebellum	**-41**	**-66**	**-42**	**>5.44**	**41**	**-66**	**-42**	**>5.44**
Main effect ISC control								
Occipital lobe								
superior occipital gyrus	-18	-82	30	>5.44	18	-82	30	>5.44
middle occipital gyrus	-34	-84	13	>5.44	34	-84	13	>5.44
inferior occipital gyrus	-36	-80	-6	>5.44	36	-80	-6	>5.44
cuneus	-5	-78	29	>5.44	5	-78	29	>5.44
calcarine fissure	8	-80	11	>5.44	-8	-80	11	>5.44
lingual gyrus	-20	-63	-3	>5.44	20	-63	-3	>5.44
fusiform gyrus	-30	-54	-14	>5.44	30	-54	-14	>5.44
Temporal lobe								
inferior temporal gyrus	-62	-50	-14	>5.44	47	-56	-10	>5.44
middle temporal gyrus	-54	-48	8	>5.44	54	-49	8	>5.44
superior temporal gyrus	-58	-18	5	>5.44	58	-18	5	>5.44
Heschl gyrus	-53	-14	10	>5.44	54	-8	7	>5.44
Limbic lobe								
temporal pole	-55	7	-6	>5.44	58	13	-5	>5.44
anterior cingulate cortex					10	38	7	5.21
median cingulate cortex					0	-27	31	>5.44
posterior cingulate cortex					0	-34	29	>5.44
hippocampus	-21	-28	-3	>5.44	23	-11	-13	>5.44
parahippocampal gyrus	-26	-36	-12	>5.44	31	-29	-16	>5.44
Parietal lobe								
superior parietal gyrus	-21	-67	52	4.71	21	-75	51	>5.44
inferior parietal gyrus	-50	-55	47	>5.44	57	-49	48	>5.44
angular gyrus	-42	-62	42	>5.44	46	-46	25	4.73
supramarginal gyrus	-63	-46	35	5.02	59	-45	25	5.25
precuneus	-20	-50	3	>5.44	3	-49	59	>5.44
Central regions								
precentral gyrus					47	7	31	>5.44
postcentral gyrus					35	-38	60	5.32
Frontal lobe								
superior frontal gyrus	-25	57	7	>5.44				
middle frontal gyrus	-28	56	7	>5.44	41	53	1	5.24
inferior frontal gyrus					56	25	21	>5.44
supplementary motor area					0	14	49	5.12
Subcortical regions								
amygdala	-23	-7	-10	5.16	24	-7	-10	>5.44
putamen	-28	-5	-7	5.17	25	3	-4	5.29
Cerebellum	**-33**	**-78**	**-22**	**>5.44**	**42**	**-57**	**-42**	**>5.44**

Table S2. Summary of regions exhibiting ISC main effects during exposure to the aversive and neutral control movie clips separately for experiment 1 (see Figs. 1A and 1B). All regions are significant at $P < .05$, whole-brain corrected. Note that 5.44 is the maximum voxel-wise permutation based z-score given 1000 permutations. Large clusters

extending across multiple brain regions are subdivided according to the Automatic Anatomical Labeling template (S*37*).

Contrast	Left Hemisphere				Right Hemisphere			
Region	x (mm)	y (mm)	z (mm)	Z	x (mm)	y (mm)	z (mm)	Z
ISC aversive > neutral								
frontoinsular cortex	-30	20	7	>5.84	37	19	4	>5.84
dorsal anterior cingulate cortex / supplementary motor area					0	0	38	>5.84
dorsolateral prefrontal cortex	-42	46	18	5.82	49	45	8	>5.84
precentral gyrus	-42	-7	57	>5.84	58	9	30	>5.84
inferior frontal / precentral gyrus	-53	6	27	>5.84	53	6	27	>5.84
medial prefrontal cortex					2	57	13	>5.84
inferior frontal gyrus (orbital)	-22	14	-21	>5.84	29	35	-14	>5.84
ventromedial prefrontal cortex					0	52	-7	>5.84
temporoparietal junction / superior parietal / supramarginal / angular gyrus	-59	-26	26		59	-26	26	>5.84
posterior cingulate cortex / precuneus					0	6	35	>5.84
superior /middle temporal gyrus	-56	-22	9	>5.84	60	-23	9	>5.84
inferior temporal gyrus	-52	-61	-9	>5.84	56	-55	-9	>5.84
parahippocampal gyrus	-21	-27	-12	4.93				
calcarine fissure	-4	-102	11	>5.84				
thalamus	-7	-16	5	>5.84	7	-16	5	>5.84
striatum / caudate nucleus					7	18	0	5.01
midbrain	-6	-26	-10	>5.84	6	-26	-10	>5.84
amygdala	-21	-4	-21	4.93				
hypothalamus					7	-7	-14	>5.84
ISC neutral > aversive								
fusiform gyrus					29	-56	-4	5.82

Table S3. Summary of regions exhibiting stronger ISC during exposure to the aversive than to the neutral control movie clip (see figure 1C), or vice versa. All reported local maxima are significant at $P < .05$, whole-brain corrected at the voxel level. Note that 5.85 is the maximum voxel-wise permutation based z-score given 10,000 permutations.

Correlation	Left Hemisphere				Right Hemisphere			
Region	x (mm)	y (mm)	z (mm)	Z	x (mm)	y (mm)	z (mm)	Z
Selected IC experiment 1								
frontoinsular cortex	-34	18	4	6.1	34	22	4	5.81
dorsal anterior cingulate cortex / supplementary motor area					2	10	40	7.27
temporoparietal junction / superior parietal / supramarginal / angular gyrus	-62	-26	36	9.99	62	-26	36	9.66
inferior/middle temporal gyrus	-54	-62	-4	5.86	54	-54	-8	4.86
thalamus	-6	-18	4	5.21	6	-18	0	5.33
precentral gyrus	-26	-6	64	5.72	26	-2	64	5.54
dorsolateral PFC	-38	42	24	4.71	34	46	28	3.93
inferior frontal / precentral gyrus	-54	6	20	6.67	54	10	12	6.36
midbrain	-7	-24	-3	4.37	7	-23	-4	4.32
amygdala	-18	-2	-16	3.04	16	2	-16	2.99
hypothalamus	-10	2	-8	3.71	10	2	-8	3.5
Selected IC experiment 2								
frontoinsular cortex	-34	18	4	5.01	42	18	0	4.84
dorsal anterior cingulate cortex / supplementary motor area	-2	10	32	5.51				
temporoparietal junction / superior parietal / supramarginal / angular gyrus	-66	-26	24	11.62	62	-22	24	11.86
inferior/middle temporal gyrus /occipital	-50	-70	0	9.32	50	-62	-4	7.73
thalamus	-10	-18	8	4.16	10	-18	8	4.07
precentral gyrus	-30	-6	60	6.87	30	-6	60	5.93
lateral PFC (dorsal/ventral)	-38	42	28	5.75	38	38	28	4.03
inferior frontal / precentral gyrus	-58	10	24	8.6	58	10	20	8.86
midbrain	-10	-30	-4	3.95				
amygdala	-26	-2	-16	3.07	18	-1	-12	2.65
hypothalamus	-10	2	8	3.74	10	2	8	4.32
(ventral) striatum / pallidum	-10	2	-4	3.18				

Table S4. Summary of regions comprising the IC maps selected using template matching for experiment 1 and 2 (see Figs. 2 and 4, respectively). Regional peaks are listed exceeding a posterior probability threshold of $P > .05$ ($Z > 1.92$) using a Gaussian/Gamma mixture model approach.

ICs exp. 1 aversive	*IC1*	***IC2***	*IC3*	*IC4*	*IC5*	*IC6*	*IC7*	*IC8*	*IC9*	*IC10*	*IC11*	*IC12*	*IC13*	*IC14*	*IC15*	*IC16*	*IC17*	*IC18*
Goodness-of-fit																		
ISC avers.>neut.	0.49	**2.02**	0.09	1.86	0.74	1.72	0.02	0.15	0.63	0.37	0.23	0.27	0.72	0.21	0.55	0.38	0.22	0.56
Prior ICN(43)	1.47	**2.89**	1.51	1.27	0.43	2.70	0.11	0.61	0.66	2.20	0.37	1.93	0.84	1.67	0.53	1.06	0.13	2.15
Subject modes																		
One sample t-test	26.7**	**20.1****	22.5**	17**	13.3**	17**	12.4**	13.8**	14.5**	9**	10.6**	6.3**	7.5**	2.7*	3.3*	3.5**	3.3**	0.8
KS Z score	0.7	**0.8**	0.7	1.0	1.2	0.9	1.2	0.7	1.6	1.6*	1.8*	1.3	1.7*	3.3**	2.6**	2.6**	2.2**	3.1**

ICs exp. 1 neutral	*IC1*	*IC2*	*IC3*	*IC4*	*IC5*	*IC6*	*IC7*	*IC8*	*IC9*	*IC10*	*IC11*	*IC12*	*IC13*	*IC14*	*IC15*	*IC16*	*IC17*
Goodness-of-fit																	
ISC avers.>neut.	0.18	0.21	0.71	0.40	0.23	0.89	0.22	0.73	0.43	0.52	0.65	1.36	1.29	0.22	0.13	0.57	0.34
Prior ICN(43)	0.35	0.39	0.81	0.08	0.10	0.73	0.45	0.31	1.34	1.88	0.35	0.85	0.23	0.64	1.42	1.34	0.50
Subject modes																	
One sample t-test	25.2**	25.8**	10**	8.4**	5**	4.3**	1.2	7.2**	6.2**	1.9	2.1*	2.1*	0.9	1.1	1.2	0.5	0.4
KS Z score	0.7	0.8	1.7*	2.2**	2.9**	2.9**	3.4**	1.9*	1.4*	3.1**	3.4**	3.1**	1.4*	4.0**	2.7**	2.8*	3.0**

ICs exp. 2 aversive	*IC1*	***IC2***	*IC3*	*IC4*	*IC5*	*IC6*	*IC7*	*IC8*	*IC9*	*IC10*	*IC11*	*IC12*	*IC13*	*IC14*	*IC15*	*IC16*
Goodness-of-fit																
Selected IC exp. 1	1.43	**5.87**	2.24	0.86	0.21	0.42	0.48	3.54	3.57	0.15	0.6	0.25	0.49	0.93	0.31	0.99
Subject modes																
One sample t-test	27.9**	**16.0****	13.6**	11.2**	17.6**	12.2**	13.7**	17.0**	17.2**	15.0**	11.9**	11.0**	8.1**	3.7**	5.6**	0.4
KS Z score	0.9	**0.7**	0.8	1.1	0.6	0.9	0.8	0.7	0.5	0.5	0.6	0.8	1.1	1.3	0.6	1.5*

Table S5. Summary of results from the template matching procedure. All IC maps resulting from ICA on the dataset from the first experiment were matched onto the ISC contrast map (aversive > control) as well as onto a template map of a previously ICN (S*43*), yielding goodness-of-fit scores (difference between average z score inside and outside of template) for each match. Also shown are t values resulting from a one sample t-test (testing whether mean subject mode of each component was above zero) and Z scores resulting from a Kolmogorov-Smirnov (KS) test for normality of the distribution (used to identify ICs carried by single individuals). ICs selected using this template matching procedure are printed in bold. Template matching for the neutral condition did not meet the criteria for success: all ICs with a match score above 1 were carried by outlier subjects (all KS $Z > 1.4$, $P < .05$) and none contained the main regions exhibiting stronger intersubject correlations for the aversive movie. For template matching of the selected ICs from experiment 1 and 2, we confirmed that the activation time courses corresponded closely ($r = .88$, $P < .001$). IC, independent component; ICN, intrinsic connectivity network; ISC, intersubject correlation; exp., experiment; avers., aversive movie condition; neut., neutral movie condition; *, $P < .05$; **, $P < .001$.

References

S1. F. S. Maheu, R. Joober, S. Beaulieu, S. J. Lupien, Differential effects of adrenergic and corticosteroid hormonal systems on human short- and long-term declarative memory for emotionally arousing material. Behav. Neurosci. 118, 420 (2004).

S2. C. D. Spielberger, R. L. Gorsuch, R. Lushene, P. R. Vagg, G. A. Jacobs, Manual for the State-Trait Anxiety Inventory. (Consulting Psychologists Press, Palo Alto, CA, 1983).

S3. A. T. Beck, A. J. Rush, B. Shaw, G. Emory, Cognitive therapy of depression. (Guilford, New York, 1979).

S4. D. Watson, L. A. Clark, A. Tellegen, Development and validation of brief measures of positive and negative affect: the PANAS scales. J. Pers. Soc. Psychol. 54, 1063 (1988).

S5. H. Cousijn et al., Acute stress modulates genotype effects on amygdala processing in humans. Proc. Natl. Acad. Sci. U. S. A. 107, 9867 (2010).

S6. M. J. A. G. Henckens, E. J. Hermans, Z. Pu, M. Joels, G. Fernandez, Stressed memories: how acute stress affects memory formation in humans. J. Neurosci. 29, 10111 (2009).

S7. L. Ossewaarde et al., Neural mechanisms underlying changes in stress-sensitivity across the menstrual cycle. Psychoneuroendocrinology 35, 47 (2010).

S8. B. A. Strange, R. J. Dolan, Beta-adrenergic modulation of emotional memory-evoked human amygdala and hippocampal responses. Proc. Natl. Acad. Sci. U. S. A. 101, 11454 (2004).

S9. B. Roozendaal, B. Mcewen, S. Chattarji, Stress, memory and the amygdala. Nat. Rev. Neurosci. 10, 423 (2009).

S10. A. M. Zardetto-Smith, T. S. Gray, Organization of peptidergic and catecholaminergic efferents from the nucleus of the solitary tract to the rat amygdala. Brain Res. Bull. 25, 875 (1990).

S11. A. H. van Stegeren, W. Everaerd, L. Cahill, J. L. McGaugh, L. J. Gooren, Memory for emotional events: differential effects of centrally versus peripherally acting beta-blocking agents. Psychopharmacology (Berl.) 138, 305 (1998).

S12. A. van Stegeren, N. Rohleder, W. Everaerd, O. T. Wolf, Salivary alpha amylase as marker for adrenergic activity during stress: effect of betablockade. Psychoneuroendocrinology 31, 137 (2006).

S13. S. Batzri, Z. Selinger, Enzyme secretion mediated by the epinephrine -receptor in rat parotid slices. Factors governing efficiency of the process. J. Biol. Chem. 248, 356 (1973).

S14. J. S. Jenkins, J. W. Meakin, D. H. Nelson, G. W. Thorn, Inhibition of adrenal steroid 11-oxygenation in the dog. Science 128, 478 (1958).

S15. S. J. Lupien et al., Acute modulation of aged human memory by pharmacological manipulation of glucocorticoids. J. Clin. Endocrinol. Metab. 87, 3798 (2002).

S16. J. Born, H. L. Fehm, K. H. Voigt, ACTH and attention in humans: a review. Neuropsychobiology 15, 165 (1986).

S17. D. Rotllant, S. Ons, J. Carrasco, A. Armario, Evidence that metyrapone can act as a stressor: effect on pituitary-adrenal hormones, plasma glucose and brain c-fos induction. Eur. J. Neurosci. 16, 693 (2002).

S18. J. W. Mason, A review of psychoendocrine research on the pituitary-adrenal cortical system. Psychosom. Med. 30, Suppl:576 (1968).
S19. J. C. Speisman, R. S. Lazarus, L. Davison, A. M. Mordkoff, Experimental analysis of a film used as a threatening stimulus. J. Consult. Psychol. 28, 23 (1964).
S20. W. Wittling, M. Pfluger, Neuroendocrine hemisphere asymmetries: salivary cortisol secretion during lateralized viewing of emotion-related and neutral films. Brain Cogn. 14, 243 (1990).
S21. V. A. Nejtek, High and low emotion events influence emotional stress perceptions and are associated with salivary cortisol response changes in a consecutive stress paradigm. Psychoneuroendocrinology 27, 337 (2002).
S22. S. Qin, E. J. Hermans, H. J. van Marle, J. Luo, G. Fernández, Acute psychological stress reduces working memory-related activity in the dorsolateral prefrontal cortex. Biol. Psychiatry 66, 25 (2009).
S23. K. Dedovic, A. Duchesne, J. Andrews, V. Engert, J. C. Pruessner, The brain and the stress axis: The neural correlates of cortisol regulation in response to stress. Neuroimage 47, 864 (2009).
S24. J. C. Pruessner et al., Deactivation of the limbic system during acute psychosocial stress: evidence from positron emission tomography and functional magnetic resonance imaging studies. Biol. Psychiatry 63, 234 (2008).
S25. J. Wang et al., Perfusion functional MRI reveals cerebral blood flow pattern under psychological stress. Proc. Natl. Acad. Sci. U. S. A. 102, 17804 (2005).
S26. S. Folkman, R. S. Lazarus, The relationship between coping and emotion: implications for theory and research. Soc. Sci. Med. 26, 309 (1988).
S27. A. Ohman, S. Mineka, Fears, phobias, and preparedness: toward an evolved module of fear and fear learning. Psychol. Rev. 108, 483 (2001).
S28. M. Davis, P. J. Whalen, The amygdala: vigilance and emotion. Mol. Psychiatry 6, 13 (2001).
S29. L. E. Goldstein, A. M. Rasmusson, B. S. Bunney, R. H. Roth, Role of the amygdala in the coordination of behavioral, neuroendocrine, and prefrontal cortical monoamine responses to psychological stress in the rat. J. Neurosci. 16, 4787 (1996).
S30. M. A. Griswold et al., Generalized autocalibrating partially parallel acquisitions (GRAPPA). Magn. Reson. Med. 47, 1202 (2002).
S31. J. C. Pruessner, C. Kirschbaum, G. Meinlschmid, D. H. Hellhammer, Two formulas for computation of the area under the curve represent measures of total hormone concentration versus time-dependent change. Psychoneuroendocrinology 28, 916 (2003).
S32. M. E. Thomason, B. E. Burrows, J. D. E. Gabrieli, G. H. Glover, Breath holding reveals differences in fMRI BOLD signal in children and adults. Neuroimage 25, 824 (2005).
S33. R. Oostenveld, P. Fries, E. Maris, J.-M. Schoffelen, FieldTrip: Open source software for advanced analysis of MEG, EEG, and invasive electrophysiological data. Comput. Intell. Neurosci. 2011, 156869 (2011).
S34. U. Hasson, Y. Nir, I. Levy, G. Fuhrmann, R. Malach, Intersubject synchronization of cortical activity during natural vision. Science 303, 1634 (2004).

S35. S. Hayasaka, T. E. Nichols, Validating cluster size inference: random field and permutation methods. Neuroimage 20, 2343 (2003).
S36. E. Maris, R. Oostenveld, Nonparametric statistical testing of EEG- and MEG-data. J. Neurosci. Methods 164, 177 (2007).
S37. N. Tzourio-Mazoyer et al., Automated anatomical labeling of activations in SPM using a macroscopic anatomical parcellation of the MNI MRI single-subject brain. Neuroimage 15, 273 (2002).
S38. C. F. Beckmann, S. M. Smith, Tensorial extensions of independent component analysis for multisubject FMRI analysis. Neuroimage 25, 294 (2005).
S39. M. J. McKeown et al., Analysis of fMRI data by blind separation into independent spatial components. Hum. Brain Mapp. 6, 160 (1998).
S40. M. J. McKeown et al., Spatially independent activity patterns in functional MRI data during the stroop color-naming task. Proc. Natl. Acad. Sci. U. S. A. 95, 803 (1998).
S41. C. F. Beckmann, M. DeLuca, J. T. Devlin, S. M. Smith, Investigations into resting-state connectivity using independent component analysis. Philos. Trans. R. Soc. Lond. B. Biol. Sci. 360, 1001 (2005).
S42. M. D. Greicius, G. Srivastava, A. L. Reiss, V. Menon, Default-mode network activity distinguishes Alzheimer's disease from healthy aging: evidence from functional MRI. Proc. Natl. Acad. Sci. U. S. A. 101, 4637 (2004).
S43. W. W. Seeley et al., Dissociable intrinsic connectivity networks for salience processing and executive control. J. Neurosci. 27, 2349 (2007).